Impacts of devegetation on the temporal evolution of soil saturated hydraulic conductivity in a vegetated sand dune area

Article *in* Environmental Earth Sciences · December 2014

DOI: 10.1007/s12665-014-3936-8

CITATIONS
3

READS
159

4 authors:

Tiejun Wang
Tianjin University
27 PUBLICATIONS **359** CITATIONS
SEE PROFILE

Erkan Istanbulluoglu
University of Washington Seattle
97 PUBLICATIONS **953** CITATIONS
SEE PROFILE

David A Wedin
University of Nebraska at Lincoln
78 PUBLICATIONS **11,268** CITATIONS
SEE PROFILE

Paul R. Hanson
University of Nebraska at Lincoln
59 PUBLICATIONS **582** CITATIONS
SEE PROFILE

Environ Earth Sci
DOI 10.1007/s12665-014-3936-8

ORIGINAL ARTICLE

Impacts of devegetation on the temporal evolution of soil saturated hydraulic conductivity in a vegetated sand dune area

Tiejun Wang · Erkan Istanbulluoglu · David Wedin · Paul Hanson

Received: 9 May 2014 / Accepted: 4 December 2014

Abstract Soil saturated hydraulic conductivity (K_S) is partly affected by vegetation activities, which can either increase K_S by enhancing macropore flow or reduce K_S by clogging pore space. Despite the complex interactions of K_S with vegetation, the impact of devegetation on K_S has not been adequately addressed, particularly in regions that are prone to drought-induced devegetation. In this study, the impacts of devegetation on K_S in a native grassland-stabilized sand dune area were investigated by artificially controlling surface vegetation at an experimental site in the Nebraska Sand Hills. The experimental results revealed that the temporal evolution of K_S at the site was mainly affected by the erosion processes triggered by devegetation. Over a short-term (about 1 year), the impact of devegetation on K_S was negligible, owing to that the existence of dead root systems prevented erosion processes. By comparison, the long-term impact of devegetation on K_S emerged when devegetation-induced erosion processes exposed deeper soil layers with higher K_S. Particularly, the dunetop locations that experienced higher erosion rates had larger temporal changes in K_S. Thus, the impacts of devegetation on K_S mainly depended on two factors (i.e., time and topographic locations) that were related to erosion processes in this native grassland-stabilized sand dune area. To further investigate the ecohydrological implications of the temporal change in K_S, a newly developed ecohydrological model was also employed, and the simulation results showed that the impacts of changes in K_S on water balance components and biomass production were non-negligible and highly nonlinear. In spite of previous studies, the findings presented here demonstrate the close tie between near-surface hydrology and land surface evolution processes controlled by vegetation in sand dune areas, and highlight the importance of coupling eco-hydro-geomorphic interactions in the context of climate change.

Keywords Saturated hydraulic conductivity · Nebraska Sand Hills · Devegetation · Erosion processes · Ecohydrology

T. Wang (✉) · D. Wedin · P. Hanson
School of Natural Resources, University of Nebraska-Lincoln, Hardin Hall, 3310 Holdrege Street, Lincoln, NE 68583, USA
e-mail: twang3@unl.edu

E. Istanbulluoglu
Department of Civil and Environmental Engineering, University of Washington, Seattle, WA, USA

Introduction

Soil saturated hydraulic conductivity (K_S) is an important soil hydraulic property that affects subsurface movements of water and solute (Amadi 2013; Zhang et al. 2013; Wang et al. 2014a; Zhou et al. 2014). The spatiotemporal variations in K_S are reflections of complex interactions among different geological, biological, hydrological, and geomorphic processes (Wösten et al. 2001; Wilcox et al. 2003; Lohse and Dietrich 2005). Among those processes, vegetation plays a pivotal role in modifying K_S through different mechanisms. Depending on vegetation types, it may either increase K_S by enhancing macropore flow due to root activities (Rasse et al. 2000; Green et al. 2003; Wilcox et al. 2003; Li et al. 2008; Lichner et al. 2011), or reduce K_S by clogging pore space (Doerr et al. 2000; Belnap et al. 2003; Yair 2003). Despite the complex interactions of K_S with vegetation, the impact of devegetation on K_S has been rarely investigated, particularly in regions with fragile ecosystems such as the Nebraska Sand Hills (NSH).

Published online: 16 December 2014

The 58,000 km^2 Nebraska Sand Hills is the largest native grassland-stabilized sand dune area in the Western Hemisphere, and poses unique ecological and hydrological importance in the region (Loope and Swinehart 2000; Wang et al. 2009a); however, severe drought-induced devegetation had caused several times of dune mobilizations in the past 10,000 years (Miao et al. 2007). Meanwhile, the high infiltration capacity of sandy soils in the region makes the NSH an important recharge area for the Ogallala aquifer and leads to a unique hydrological system driven by groundwater (Bleed and Flowerday 1998; Istanbulluoglu et al. 2012a). To understand the spatial distribution patterns of K_S in the NSH, Wang et al. (2008) analyzed the effects of depth and topographic positions on K_S, and found that K_S was significantly correlated with both depth and elevation. Wang et al. (2009b) further indicated that vegetation in the NSH may affect K_S through altering soil organic matter contents. However, given the vulnerability of the NSH to devegetation and subsequent destabilizations, it still remains unclear about which processes would affect the temporal evolution of K_S during the process of devegetation, which may have important ecohydrological implications for the NSH under climate change conditions.

To this end, field campaigns were carried out to measure in situ K_S at an experimental site in the NSH, at which surface vegetation was artificially controlled. The objectives of this study were twofold. The first goal was to investigate the dominant mechanisms, through which devegetation affected K_S in the NSH. Second, to evaluate the ecohydrological implications induced by changes in K_S due to devegetation, a newly developed ecohydrological model was employed to simulate water balance and biomass production in the NSH.

Materials and methods

Study site

This study was conducted at the Grassland Destabilization EXperiment (GDEX) site in the eastern NSH (42°14′N, 99°39′W), which was constructed to investigate the ecological and geomorphic stability of the sand dunes in the NSH. The detailed information on the study site and the experimental designs can be found elsewhere (Wang et al. 2008; http://snr.unl.edu/sandhills-biocomplexity/index.htm), and only a brief overview is given here. The local climate is semiarid with mean annual precipitation of 576 mm year^{-1}. The landscape is mainly composed of sand dunes covered by native warm season (C4) grasses with aboveground biomass productivities ranging from 200 to 400 g m^{-2} year^{-1} (Istanbulluoglu et al. 2012b). Surface soils in the top 10 cm are sandy at both ridges and swales with average sand contents of 94.4 and 91.2 %, respectively. Beneath 10 cm depths, average sand contents slightly increase up to 97 %, regardless of topographic positions. Soils are classified either as the Valentine series, a mixed, mesic Typic Udipsamments that lacks any diagnostic subsurface horizon, or where A horizon exceeds 25 cm, as the Dunday series, a sandy, mixed, mesic Entic Haplustolls with a diagnostic mollic epipedon. Optically stimulated luminescence dating of the dune sediments in the area indicated that the upper 5–7 m of the dunes were typically 700–900 years old, suggesting the approximate time of the last dune destabilization in the region (Miao et al. 2007).

Ten circular plots, each with 120 m in diameter, were constructed at the GDEX site. To study the impact of vegetation on dune stability, vegetation covers were experimentally controlled at the GDEX site. Among those plots, Plot 2 was used as a control plot and represented natural conditions without any disturbances (e.g., grazing), vegetation at Plot 7 was completely removed by herbicide and raking in May 2004, and vegetation at Plot 8 was also killed by herbicide but left intact since May 2005. In addition, erosion pins were installed at Plot 7 and Plot 8 to monitor surface erosion rates at different topographic locations.

In-situ measurements of K_S

In-situ K_S at the depths of 20, 50, and 100 cm was measured using a compact constant-head permeameter (Amoozegar 1989a; Fig. 1). The permeameter maintained a constant water head in a borehole and measured the

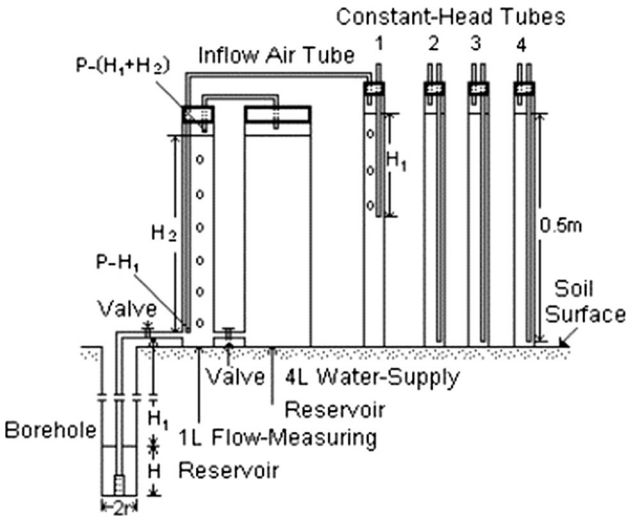

Fig. 1 Schematic of the compact constant-head permeameter used for measuring saturated hydraulic conductivity in this study (modified from Amoozegar 1989a)

discharge rate from the borehole into the surrounding soils. The discharge rate was then used to calculate in situ K_S based on the well-established solution of Glover (1953), (Amoozegar 1989b; Stephens 1996):

$$K_S = \frac{Q}{2\pi H^2}\left\{\sinh^{-1}(H/r) - \left[1 + (r/H)^2\right]^{0.5} + r/H\right\} \quad (1)$$

where Q [L^3T^{-1}] is the steady infiltration rate, r [L] is the borehole radius, and H [L] is the water depth in the borehole. A hand auger with 5 cm in diameter was used to construct the borehole and a flat-bottom auger was then used to complete the borehole by carefully shaving the borehole bottom (Amoozegar 1989a; Wang et al. 2008). In each borehole, the K_S measurements were repeated three times at each depth (e.g., 20, 50, and 100 cm), and the average values of the three K_S measurements at each depth were used for the following analysis. The same protocol for measuring K_S was used for all the field campaigns in this study.

To investigate the short-term and long-term effects of devegetation on K_S at the GDEX site, two major field campaigns were carried out to measure in situ K_S. The first campaign was undertaken in June 2005, which was approximately, 1 year after removing the vegetation cover at Plot 7 and 1 month after killing the vegetation cover at Plot 8. The second campaign took place about 4 years after the first one in July 2009. During the 2005 campaign, K_S was measured along the ridge of Plot 7, and the ridges and swales of Plot 2 and Plot 8. Note that due to the irregular shape of the sand dune at Plot 7, K_S was only measured along its ridge. It led to a total of 28 K_S profiles with 10 profiles at Plot 2, 7 at Plot 7, and 11 at Plot 8 (Table 1). In the 2009 campaign, a total of 19 K_S profiles were taken with 6 profiles at Plot 2, 7 at Plot 7, and 6 at Plot 8 (Table 1). Along each transect, the distance between neighboring boreholes was approximately, 20 m. It should be stressed that the borehole locations between the two campaigns were not at the exactly same locations due to the changing morphology of the sand dunes; however, it would not change the conclusions made in this study.

Table 1 Number of K_S profiles measured during each field campaign

Plot	Year	Number of sampling profiles	
		Ridge	Swale
Plot 2	2005	5	5
	2009	3	3
Plot 7	2005	7	–
	2009	8	–
Plot 8	2005	6	5
	2009	3	3

Ecohydrological model

To assess the ecohydrological implications of changes in K_S, a newly developed ecohydrological model was employed to simulate water balance and biomass production (Istanbulluoglu et al. 2012b). The model mainly consists of a hydrological and a dynamic vegetation component. For the hydrological component, a point-scale water balance model is used (Laio et al. 2001):

$$nZ_r\frac{ds}{dt} = I_a - ET_a(s) - D(s) \quad (2)$$

where n [−] is porosity, Z_r [L] is effective rooting depth, s [−] is saturation degree of soil moisture, t [T] is time, I_a [LT^{-1}] is infiltration rate, ET_a [LT^{-1}] is actual evapotranspiration rate, and D [LT^{-1}] is drainage rate. For the infiltration process, I_a is set to be the smaller value between rainfall intensity or soil infiltration capacity when soil is unsaturated, or to be equal to the drainage rate D when soil becomes saturated. At the lower boundary of the root zone, the unit hydraulic gradient assumption is applied:

$$D(s) = \begin{cases} K_S & s = 1 \\ K(s) = K_S s^{(2b+3)} & s_{fc} < s \le 1 \end{cases}. \quad (3)$$

where $K(s)$ [LT^{-1}] is unsaturated hydraulic conductivity depending on s, b [−] is an empirical parameter in the Campbell retention model (Campbell 1974), and s_{fc} is saturation degree at the field capacity. The drainage rate D is assumed to be zero, when s is smaller than s_{fc} (Laio et al. 2001).

The actual evapotranspiration rate ET_a is calculated as:

$$ET_a = ET_p \cdot \beta_s(s) \quad (4)$$

where ET_p [LT^{-1}] is potential evapotranspiration. The parameter β_s [−] represents the effect of soil moisture on transpiration and evaporation (Laio et al. 2001):

$$\beta_s(s) = \begin{cases} 0, & s_h < s \le s_w \\ \dfrac{s - s_w}{s* - s_w}, & s_w < s \le s^* \\ 1 & s^* < s \end{cases} \quad (5)$$

where s_h is saturation degree at the soil hygroscopic capacity, and s_w and s^* are saturation degrees corresponding to plant water potentials at the wilting point and incipient stomata closure, respectively.

The vegetation dynamic module simulates daily net primary production (NPP, g DM m^{-2} d^{-1}), and its allocation between aboveground and belowground biomass pools. The daily net primary production NPP is calculated as (Sitch et al. 2003; Williams and Albertson 2005): where WUE is water use efficiency with units of kg CO_2 kg^{-1} H_2O, ρ_v [ML^{-3}] is water density, w is a factor converting CO_2 to dry matter with units of kg DM kg^{-1} CO_2, and μ [−

] is the ratio of nighttime to daytime CO_2 exchange and assumed to be 0.4 (Williams and Albertson 2005). The annual NPP of the ecosystem (ANPP) is defined as the maximum NPP during a year. The onsets of growing (GT: growth threshold) and dormancy (DT: dormancy threshold) seasons are dictated by a 30-day running average of ET_p, which is used as a surrogate for climatic conditions that control the growth of vegetation.

The growth and decay of aboveground (i.e., B_g) and belowground (i.e. B_r) biomass are described by a commonly used first-order kinetic growth model. More specifically, NPP is partitioned between B_g and B_r using an allocation coefficient α that depends on available space (Williams and Albertson 2005):

$$\frac{dB_g}{dt} = \text{NPP} \times \alpha - k_{sg}B_g \quad (7)$$

$$\frac{dB_r}{dt} = \text{NPP} \times (1-\alpha) - k_{sr}B_d \quad (8)$$

$$\frac{dB_r}{dt} = k_{sg}B_g - k_{dd}\gamma B_r \quad (9)$$

where B_d is dead biomass, k_{sg}, k_{sr}, and k_{dd} are decay coefficients for aboveground, root, and dead biomass, respectively, and γ is the dead biomass loss rate.

Results and discussions

Comparison of short-term and long-term effects of devegetation on K_S

To have an overall view of the short-term and long-term effects of devegetation on K_S, the profiles of average K_S at each plot for 2005 and 2009 are shown in Fig. 2. In general, there was a twofold increase in K_S from the depth of 20–100 cm at all the plots in both 2005 and 2009. The increasing trend in K_S with depth is consistent with the results of Wang et al. (2008). However, the spatial variability in K_S among different plots was considerably lower in 2005 than in 2009, which demonstrates the different impacts of the short-term and long-term devegetation on the temporal changes in K_S. Compared to K_S at the control plot (i.e., Plot 2), K_S at the disturbed plots (i.e., Plot 7 and Plot 8) showed similar ranges. Particularly, at the 20 cm depth, the spatial variability in K_S was smallest among different plots in 2005, indicating that initial conditions at the 20 cm depth before the treatments were similar at the site and the short-term effects of devegetation on K_S at Plot 7 and Plot 8 were insignificant; otherwise, one would anticipate that the short-term effects of devegetation on K_S should be the most pronounced at the 20 cm depth where most of the root biomass loss occurred, and consequently that the spatial variability in K_S should be highest at the 20 cm depth [see Wang et al. (2008) for detailed analysis of the short-term effect]. As pointed out by Wang et al. (2008), the native grasses in the NSH tend to horizontally homogenize K_S, which is different from most semi-arid landscapes where heterogeneous vegetation interacts with topographic and soil variability to create complex mosaic infiltration and runoff patterns (Wilcox et al. 2003; Ludwig et al. 2005). With a negligible effect of the short-term devegetation on K_S, K_S at the control and disturbed plots remained similar in 2005.

By comparison, the results of K_S from the 2009 campaign intuitively revealed two marked long-term impacts of devegetation on K_S. First, K_S appeared to be more spatially heterogeneous among different plots in 2009. Especially at Plot 7, with the most pronounced vegetation disturbance, K_S at all the depths became significantly different from those at the control plot (Fig. 2b). Second, K_S at all the depths increased at both Plot 7 and Plot 8 from 2005 and 2009. To further show the temporal increases in K_S at the disturbed plots, the average K_S profiles of 2005 and 2009 are compared in Fig. 3 for each plot. It can be seen from Fig. 3 that at the control plot, there was no consistent pattern of the temporal changes in K_S at different depths;

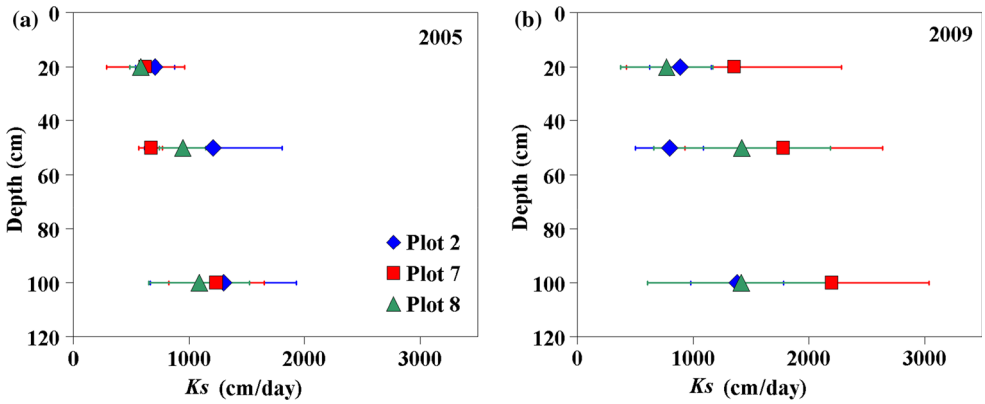

Fig. 2 Profiles of average K_S with standard deviations (*horizontal bars*) at different plots in **a** 2005 and **b** 2009

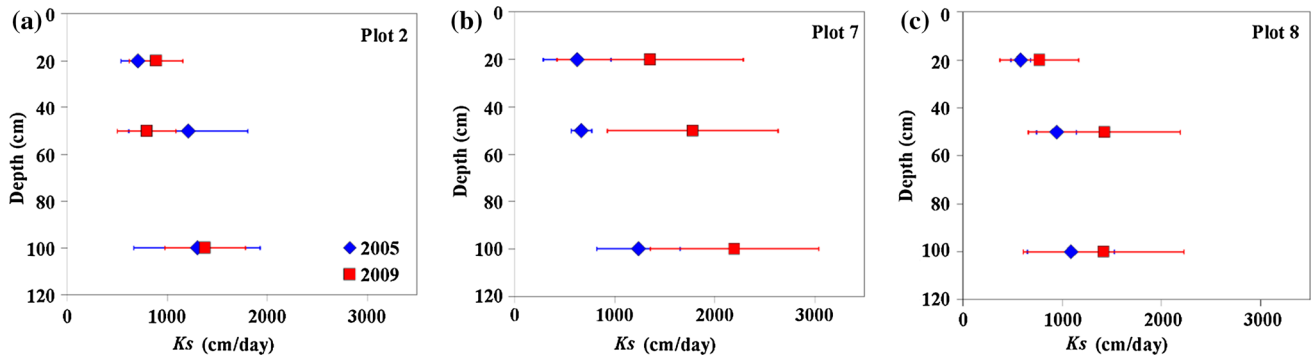

Fig. 3 Comparisons of K_S profiles measured in 2005 and 2009 at **a** Plot 2 with no vegetation disturbance, **b** Plot 7 with the vegetation cover completely removed, and **c** Plot 8 with the dead vegetation cover left intact

Table 2 Results of the nonpaired t test for the differences in K_S between 2005 and 2009

Depth (cm)	Plot 2	Plot 7	Plot 8
20	$t = 1.630$, $p = 0.127$ insignificant	$t = 1.527$, $p = 0.151$ insignificant	$t = 1.503$, $p = 0.154$ insignificant
50	$t = 1.443$, $p = 0.173$ insignificant	$t = 3.429$, $p = 0.005$ significant	$t = 2.006$, $p = 0.063$ insignificant
100	$t = 0.235$, $p = 0.818$ insignificant	$t = 2.538$, $p = 0.028$ significant	$t = 1.100$, $p = 0.289$ insignificant

whereas, K_S systematically increased at all the depths at the disturbed plots from 2005 to 2009.

The nonpaired t test was also performed to test the differences in K_S between 2005 and 2009, and the results are reported in Table 2. Before performing the nonpaired t test, the Kolmogorov–Smirnov test confirmed the normal distributions of K_S data. Although K_S largely shows log-normal distributions in agricultural soils (e.g., Rienzner and Gandolfi 2014), the results of normal distributions of K_S in this study are consistent with previous reports for coarse-textured geological materials (Chen et al. 2014; Wang et al. 2014b). As expected, at Plot 2 with no vegetation disturbance, the temporal changes in K_S from 2005 to 2009 were smallest and insignificant. In comparison, Plot 7 experienced the largest temporal changes in K_S, particularly, at the 50 cm depth ($t = 3.429$ and $p = 0.005$) and the 100 cm depth ($t = 2.538$ and $p = 0.028$). On average, K_S at Plot 7 increased from 2005 to 2009 by 92 % (from 620 to 1,190 cm day^{-1}), 167 % (from 670 to 1,790 cm day^{-1}), and 78 % (from 1240 to 2,200 cm day^{-1}) at the depths of 20, 50, and 100 cm, respectively. At Plot 8 with an intermediate vegetation disturbance, K_S exhibited modest increases with respective 32, 51, and 30 % increases at the depths of 20, 50, and 100 cm; however, the increases in K_S were not statistically significant. Nevertheless, the experimental results revealed an interesting pattern that the removal of vegetation covers at the GDEX site led to increased K_S, which resulted in higher spatial heterogeneity of K_S. This obviously contradicts with the traditional notion that vegetation increases K_S through root activities (Wilcox et al. 2003). Figure 2 thus suggests that devegetation might have affected K_S through other mechanisms at the GDEX site.

Effects of devegetation on K_S at different topographic locations

Besides the effect of depth, Wang et al. (2008) also showed that K_S at dunetop locations was generally higher than those in the interdunal areas. It is thus necessary to differentiate the impacts of devegetation on K_S at different topographic locations. Figure 4 shows the average K_S profiles in the swales of Plot 2 and Plot 8 for 2005 and 2009. Note that due to the irregular shape of the sand dune, K_S was only measured along the ridge of Plot 7. Similar to the overall pattern at Plot 2 (Fig. 3a), there was also no consistent pattern of the temporal changes in K_S in the swale of Plot 2 at different depths. More interestingly, only very subtle changes in K_S occurred in the swale of Plot 8 from 2005 to 2009 (Fig. 4b), which is different from the K_S pattern shown in Fig. 3c and implies a very limited impact of devegetation on K_S.

By comparison, the average K_S profiles at the ridges of Plot 2 and Plot 8 are plotted in Fig. 5 for 2005 and 2009. For the purpose of simplicity, the results of K_S from the ridge of Plot 7 are not shown here and can be found in Fig. 3b. Apparently, K_S at the ridges was generally higher than those in the swales, which is in line with the results of Wang et al. (2008). The temporal changes in K_S at the ridge of Plot 2 were similar to the ones in the swale. However, a

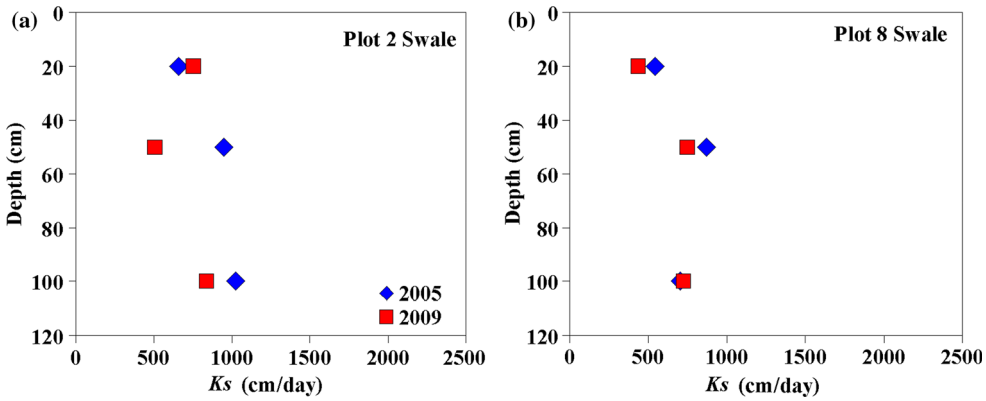

Fig. 4 Comparisons of K_S profiles measured in 2005 and 2009 in the swales of **a** Plot 2 and **b** Plot 8

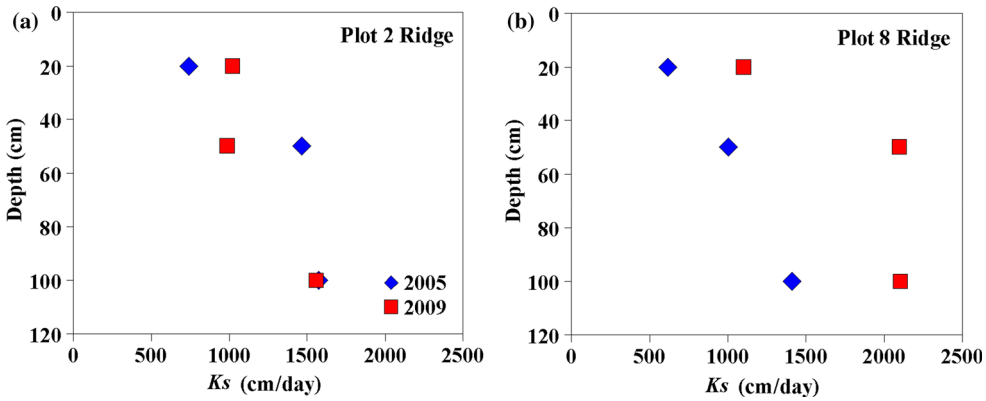

Fig. 5 Comparisons of K_S profiles measured in 2005 and 2009 at the ridges of **a** Plot 2 and **b** Plot 8

different pattern of K_S emerged at the ridge of Plot 8 compared to the ones in the swale. Figure 5b shows that K_S at the ridge of Plot 8 increased significantly from 2005 to 2009 at all the depths. On average, K_S at the ridge of Plot 8 increased from 2005 to 2009 by 79 % (from 610 to 1,790 cm day^{-1} with $t = 4.503$ and $p = 0.003$), 109 % (from 1,000 to 2,100 cm day^{-1} with $t = 6.326$ and $p < 0.001$), and 50 % (from 1,400 to 2,100 cm day^{-1} with $t = 3.503$ and $p = 0.010$) at the depths of 20, 50, and 100 cm, respectively. The temporal evolution pattern of the increased K_S at the ridge of Plot 8 was consistent with the one observed at the ridge of Plot 7 (Fig. 3b). This indicates that the long-term effect of devegetation on K_S at the GDEX site also depended on topographic positions with dunetop locations experiencing larger impacts.

Impacts of devegetation-induced erosion processes on the spatiotemporal changes in K_S

The previous sections showed that the impacts of devegetation on K_S at the GDEX site mainly depended on two factors, including time (i.e., short-term vs. long-term) and topographic location (i.e., ridge vs. swale). To further explore the underpinning processes that caused the contrasting temporal evolution patterns of K_S at different topographic locations, the spatiotemporal patterns of K_S are compared to the erosion processes at the GDEX site. Figure 6 shows the changes in elevation at Plot 7 and Plot 8 from May 2004 to June 2009, which were interpolated from 52 pins in Plot 7 and 54 pins in Plot 8. In addition, the approximate K_S survey lines are also superimposed in Fig. 6. Note that the borehole locations in the 2009 campaign were not at the exactly same locations, at which K_S was measured during the 2005 campaign, and therefore, no regression model was developed to correlate the temporal changes in K_S to the changes in elevations. Nevertheless, the contrasting temporal evolution patterns of K_S at different topographic locations can be explained by the erosion processes occurred at the GDEX site.

At the disturbed plots, surface sandy soils were eroded away by wind due to the absence of vegetation and loss of root biomass, which led to significant redistributions of surface sandy particles at those two plots as illustrated in Fig. 6. However, until the first field campaign in June 2005, only minimal sand movements occurred at Plot 7 and Plot 8 with less than 2 cm of removal or deposition of sand particles, and the soil horizons were largely intact due to the existence of dead root residues (Wang et al. 2008). At the same time, no significant differences in K_S could be observed between the control plot and the disturbed plots,

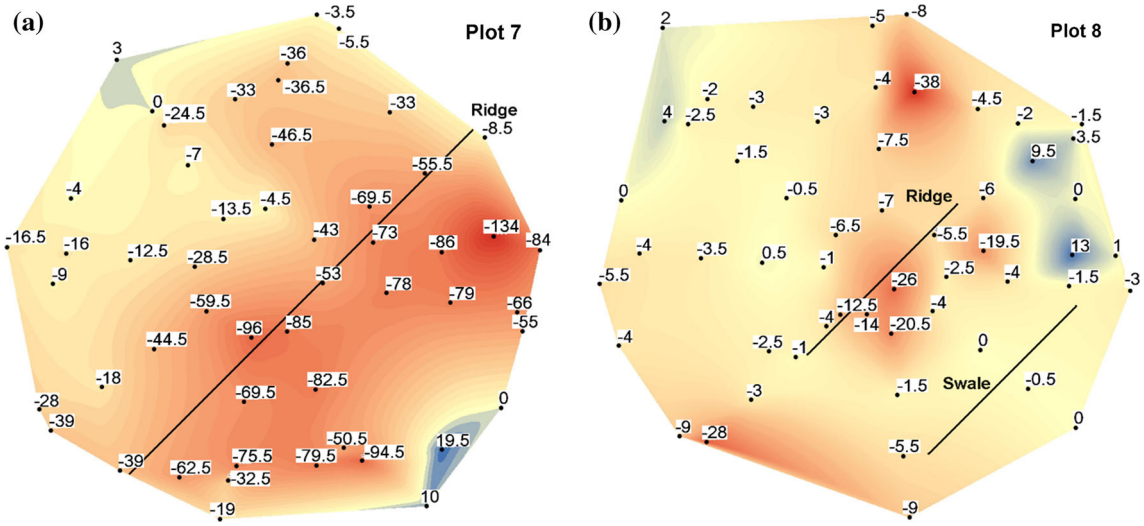

Fig. 6 Spatially interpolated maps of erosion rates at **a** Plot 7 and **b** Plot 8. Units are in cm with negative values indicating removal and positive values indicating deposition of sandy particles. *Black dots* are the locations of erosion pins and *black lines* represent the approximate K_S *survey lines*

indicating that the short-term impact of devegetation on K_S was insignificant. With the continuous decomposition of dead root biomass, however, the erosion rates accelerated significantly after 2006 at Plot 7 and Plot 8. Due to different levels of vegetation disturbances, Plot 7 exhibited much higher erosion rates than Plot 8. Moreover, it can be seen from Fig. 6 that erosion rates were significantly higher at the dunetop positions along the ridges than in the interdunal areas along the swales. By comparing the spatio-temporal patterns of K_S to the erosion rates at different topographic locations, it appears that locations with the most significant temporal changes in K_S were associated with those that experienced the largest erosion rates (i.e., ridges).

More specifically, with the highest erosion rates along the ridge of Plot 7, K_S exhibited the largest temporal changes from 2005 to 2009. Interestingly, in the swale of Plot 8, the total erosion rates were still small until May 2009, while only very subtle temporal changes in K_S occurred (Fig. 4b). In comparison, the ridge of Plot 8 received modest erosion rates and experienced modest increases in K_S. It becomes clear that depending on time and topographic locations, the erosion processes triggered by the removal of vegetation covers exposed deeper soil layers with higher K_S at the GDEX site. To further examine whether the erosion processes affected the temporal changes in K_S by removing top soil layers, a nonpaired t test was performed to compare K_S from different depths at Plot 7 (i.e., K_S at 100 cm in 2005 vs. K_S at 20 cm in 2009) and at the ridge of Plot 8 (i.e., K_S at 50 cm in 2005 vs. K_S at 20 cm in 2009), according to the erosion rates at those two plots (Fig. 6). The results showed no significant differences in K_S at Plot 7 ($t = 2.228$ and $p = 0.900$) and at the ridge of Plot 8 ($t = 3.182$ and $p = 0.220$), which indicated that the erosion processes did not affect the temporal changes in K_S through modifying soil properties in shallow soil layers. Overall, the result highlights the importance of coupling eco-hydro-geomorphic interactions to study the temporal evolution of K_S in sand dune areas.

Ecohydrological impacts of temporal changes in K_S

As an important soil hydraulic property that controls subsurface movements of water and solute, temporal changes in K_S may have important implications for the ecohydrological system in the NSH. As pointed out by Wang et al. (2009a), spatial variations in K_S significantly controlled the regional water balances in the NSH. To investigate the ecohydrological implications of temporal changes in K_S, the model developed by Istanbulluoglu et al. (2012b) described in "Ecohydrological model" was used to evaluate the impacts of K_S on water balance and biomass production in the NSH. The values of soil hydraulic parameters for sandy soils and physiological parameters for grass were taken from the literature and used in this study (Table 3; Clapp and Hornberger 1978; Laio et al. 2001; Williams and Albertson 2004, 2005; Istanbulluoglu et al. 2012b), except for K_S. In addition, the effective rooting depth Z_r was set to be 50 cm, as Wang et al. (2009b) showed that over 90 % of the total root biomass occurred in the top 50 cm at the GDEX site, which was consistent with literature reviews on the occurrence of root biomass in native grasslands (Jackson et al. 1996; Schenk and Jackson 2002). Therefore, to be consistent with the rooting depth of

Table 3 Soil and physiological parameter values used in the simulations

Parameter	Description	Value
n	Porosity	0.35
b	Empirical parameter in the Campbell model	4.05
s_{fc}	Saturation degree at field capacity	0.35
s^*	Saturation degree at stomata closure	0.33
s_w	Saturation degree at wilting point	0.09
s_h	Saturation degree at soil hygroscopic capacity	0.08
Z_r	Effective rooting depth (cm)	50
WUE	Water use efficiency (kg CO_2 kg^{-1} H_2O)	0.01
μ	Ratio of nighttime to daytime CO_2 exchange	0.4
w	Factor converting CO_2 to dry matter (kg DM kg^{-1} CO_2)	0.55
k_{sg}	Decay factor for live biomass (1 day^{-1})	0.012
GT	Growth threshold (cm day^{-1})	0.38
DT	Dormancy threshold (cm day^{-1})	0.68

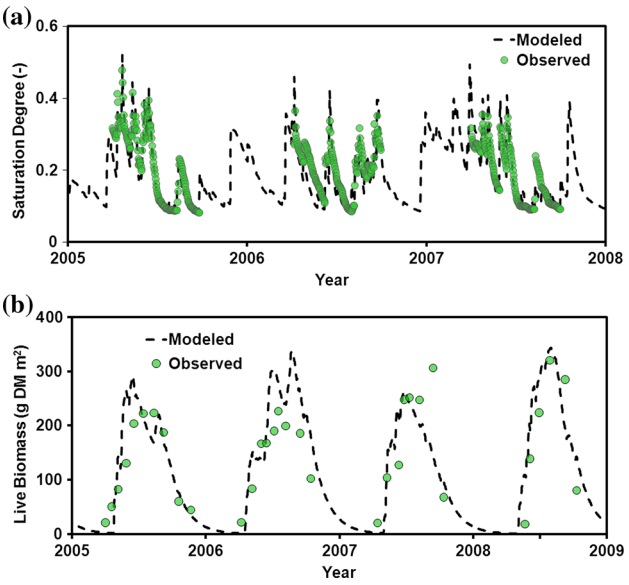

Fig. 7 Comparisons of field observations to the simulation results of the calibrated ecohydrological model for **a** soil moisture content and **b** live biomass

Z_r, average K_S values measured in the top 50 cm were used for calibrating the model and for the rest of the simulations. To be more specific, after the model was calibrated to the field observations at the GDEX site, two sets of simulations were performed with different K_S values. For the first set of simulations, K_S was set to be 600 cm day^{-1} (e.g., at Plot 2) that represented pre-treatment conditions, while for the second set of simulations, K_S was set to be 1,500 cm day^{-1} (e.g., at Plot 7) that represented post-treatment conditions.

To calibrate the model, K_S was first set to be 600 cm day^{-1}, and the vegetation decay parameter for live biomass (i.e., k_{sg}) and the two phenological parameters (i.e., GT and DT) were varied to match the observed and simulated soil moisture content and live biomass in Plot 2. The detailed calibration procedure is given in Istanbulluoglu et al. (2012b), and calibrated values of those physiological and phenological parameters are also reported in Table 3. The simulation results of the calibrated model are plotted in Fig. 7. Due to the malfunctioning of soil moisture probes, soil moisture data during winter seasons were discarded for the calibration. In general, the model was able to reproduce daily soil moisture contents reasonably well and capture most of the drainage processes. The model also successfully simulated the biomass production, particularly, the onsets of the growing and dormancy seasons as well as the timing of the peak biomass. Overall, the simulated soil moisture content and live biomass were in good agreement with the field data.

After the calibration, the model was then run for 2,000 years for each set of simulations using generated climatic data to assess the impacts of changes in K_S on the long-term water balance and biomass production. Based on current climatic conditions in the region surrounding the GDEX site, daily precipitation P was generated according to the method of Chow (1964) and daily potential evapotranspiration ET_p was generated using a cosine function adopted by Istanbulluoglu et al. (2012b). In this study, no shifts in climatic conditions from the current ones were considered, as it was still unclear about the climatic conditions, under which devegetation-induced erosion processes would occur. The simulation results for $K_S = 600$ cm day^{-1} and $K_S = 1{,}500$ cm day^{-1} are reported in Table 3, including mean annual ANPP ($\overline{ANPP}$), and the ratios of mean annual actual evapotranspiration over precipitation ($\overline{ET_a}/\overline{P}$) and mean annual drainage over precipitation ($\overline{D}/\overline{P}$). Note that the surface runoff ratio (not shown here) was less than 0.1 % in the water balances, which is consistent with the results of Wang et al. (2009c) who investigated different components of the hydrological fluxes at the GDEX site. The annual water balance components (e.g., actual evapotranspiration and drainage) were primarily dependent on annual P and ET_p levels (Wang et al. 2009a; Istanbulluoglu et al. 2012a). As such, the impact of K_S on those water balance components can be easily overridden by that of the interannual variability in P and ET_p. Over the long-term, however, the impact of K_S emerged. With a 2.5-fold increase in K_S from 600 to 1,500 cm day^{-1}, the $\overline{ET_a}/\overline{P}$ ratio dropped from 0.81 to 0.77 and the $\overline{D}/\overline{P}$ ratio increased from 0.19 to 0.23, which represented an important shift in the hydrological cycle in this semi-arid region (Wang et al. 2009a). With less available soil moisture caused by higher drainage rates, $\overline{ANPP}$ decreased from 356.39 to 351.54 g DM m^{-2} $year^{-1}$.

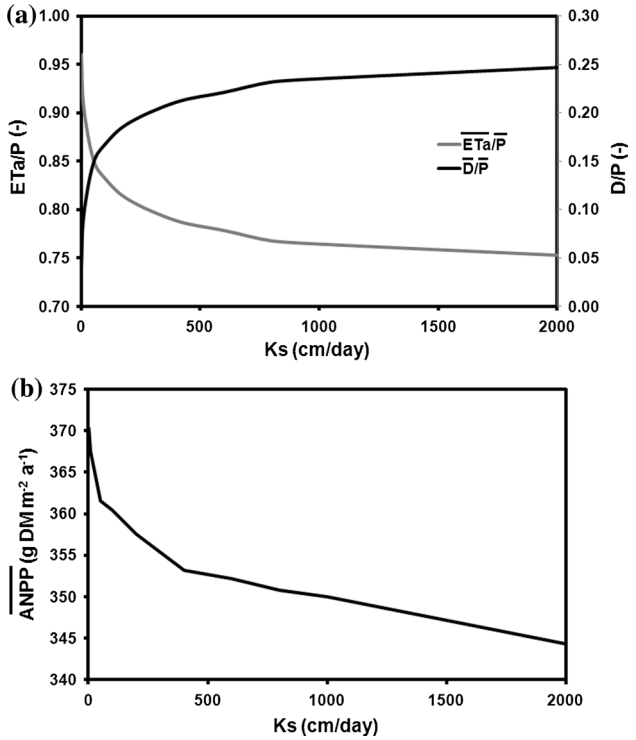

Fig. 8 Relationships of K_S with **a** mean annual water balance components ($\overline{ET_a}/\overline{P}$ and $\overline{D}/\overline{P}$), and **b** mean annual net primary production ($\overline{ANPP}$)

Table 4 Simulation results of long-term water balance and biomass production with different K_S values

K_S (cm day^{-1})	$\overline{ET_a}/\overline{P}$	$\overline{D}/\overline{P}$	$\overline{ANPP}$ (g DM m^{-2})
600	0.802	0.198	356.39
1,500	0.777	0.223	351.54

As K_S may vary significantly across the NSH (Wang et al. 2009a), it was thus imperative to further examine the impacts of K_S on water balance and biomass production with a wider range of K_S. To this end, K_S was varied from 1 to 2,000 cm day^{-1} in the calibrated model. The range of K_S values was typical for sandy soils (Schaap and Leij 1998; Wang et al. 2009c). For each K_S value, the calibrated model was also run for 2,000 years and the results are plotted in Fig. 8, which reveal two marked impacts of K_S on the long-term water balance and biomass production. First, the dependence of $\overline{ET_a}/\overline{P}$, $\overline{D}/\overline{P}$, and $\overline{ANPP}$ on K_S was highly nonlinear. At the lower range of K_S (e.g., $K_S < 1{,}000$ cm day^{-1}), the ratios of $\overline{ET_a}/\overline{P}$, $\overline{D}/\overline{P}$, and $\overline{ANPP}$ were more sensitive to the changes in K_S. Second, the impacts of K_S on water balance components were relatively larger than on biomass production. For instance, with K_S increasing from 1 to 2,000 cm day^{-1}, the $\overline{ET_a}/\overline{P}$ ratio decreased by 20.8 %, while the $\overline{ANPP}$ only decreased by 7 % (Table 4). However, this finding may not hold under climate change conditions, as vegetation growth may cease under very dry conditions.

Conclusions

In this study, by controlling vegetation covers at an experimental site in a native grassland-stabilized sand dune area, the short-term (about 1 year) and long-term (about 5 years) impacts of devegetation on K_S were investigated. The results showed that the impacts of devegetation on K_S mainly depended on two factors (i.e., time and topographic locations), both of which were related to erosion processes. Overall, the short-term impact of devegetation on K_S was negligible, owing to that the existence of dead root systems prevented erosion processes; however, with the accelerated decomposition of dead root biomass and subsequent erosion processes, the long-term impact emerged. Particularly, the dunetop locations that experienced higher erosion rates had larger temporal changes in K_S. By exposing deeper soil layers with higher K_S, devegetation-induced erosion processes largely controlled the temporal evolution of K_S in this native grassland-stabilized sand dune area. As such, the spatiotemporal patterns of K_S in sand dune areas might be a reflection of complex eco-hydro-geomorphic interactions. To investigate the ecohydrological implications of the change in K_S, an ecohydrological model was used, and the simulation results revealed that the impacts of K_S on water balance components and biomass production were highly nonlinear. Moreover, the impacts of K_S on water balance components were shown to be relatively larger than on biomass production. The findings presented in this study demonstrate the close tie between near-surface hydrology and land surface evolution processes controlled by vegetation, and highlight the importance of coupling eco-hydro-geomorphic interactions in the context of climate change (Istanbulluoglu 2009).

Acknowledgments The authors would like to thank O. Yetemen (UW) for helping with the field experiments and V. Zlotnik (UNL) for reviewing the paper, and two anonymous reviewers for their comments that led to the improvement of this work.

References

Amadi AA (2013) Swelling characteristics of compacted lateritic soil–bentonite mixtures subjected to municipal waste leachate contamination. Environ Earth Sci 70:2437–2442

Amoozegar A (1989a) A compact constant-head permeameter for measuring saturated hydraulic conductivity of the vadose zone. Soil Sci Soc Am J 53:1356–1361

Amoozegar A (1989b) Comparison of the Glover solution with the simultaneous equation approach for measuring hydraulic conductivity. Soil Sci Soc Am J 53:1362–1367

Belnap J, Prasse R, Harper KT (2003) Influence of biological soil crusts on soil environments and vascular plants. In: Belnap J, Lange OL (eds) Biological soil crusts: structure, function, and management, 2nd edn. Springer, Berlin, pp 281–300

Bleed AS, Flowerday CA (1998) An Atlas of the Sand Hills. Conservation and Survey Division, University of Nebraska-Lincoln, Lincoln, Nebraska

Campbell GS (1974) A simple method for determining unsaturated conductivity from moisture retention data. Soil Sci 117:3311–3314

Chen X, Mi H, He H, Liu R, Gao M, Huo A, Cheng D (2014) Hydraulic conductivity variation within and between layers of a high floodplain profile. J Hydrol 515:147–155

Chow VT (1964) Handbook of applied hydrology. McGraw-Hill, New York

Clapp RB, Hornberger GM (1978) Empirical equations for some hydraulic properties. Water Resour Res 14:601–604

Doerr SH, Shakesby RA, Walsh RPD (2000) Soil water repellency: its causes, characteristics and hydro-geomorphological significance. Earth Sci Rev 51:33–65

Glover RE (1953) Flow for a test hole located above groundwater level. In: Zangar CN (ed), Theory and Problems of Water Percolation. Engineering Monograph, 8, US Bureau of Reclamation, p 60

Green TR, Ahujaa LR, Benjamin JG (2003) Advances and challenges in predicting agricultural management effects on soil hydraulic properties. Geoderma 116:3–27

Istanbulluoglu E (2009) An Eco-hydro-geomorphic perspective to modeling the role of climate in catchment evolution. Geogr Compass. doi:10.1111/j.1749-8198.2009.00229.x

Istanbulluoglu E, Wang TJ, Wright OM, Lenters JD (2012a) Interpretation of hydrologic trends from a water balance perspective: the role of groundwater storage in the Budyko hypothesis. Water Resour Res 48:WOOH16

Istanbulluoglu E, Wang TJ, Wedin D (2012b) Evaluation of ecohydrologic model parsimony at local and regional scales in a semiarid grassland ecosystem. Ecohydrology 5:121–142

Jackson RB, Canadell J, Ehleringer JR, Mooney HA, Sala OE, Schulze ED (1996) A global analysis of root distributions for terrestrial biomes. Oecologia 108:389–411

Laio F, Porporato A, Ridolfi L, Rodriguez-Iturbe I (2001) Plants in water controlled ecosystems: active role in hydrological processes and response to water stress II. Probabilistic soil moisture dynamics. Adv Water Resour 24:707–723

Li XY, Contreras S, Solé-Benet A (2008) Unsaturated hydraulic conductivity in limestone dolines: influence of vegetation and rock fragments. Geoderma 145:288–294

Lichner L, Eldridge DJ, Schacht K, Zhukova N, Holko L, Šír M, Pecho J (2011) Grass cover influences hydrophysical parameters and heterogeneity of water flow in a sandy soil. Pedosphere 21:719–729

Lohse KA, Dietrich WE (2005) Contrasting effects of soil development on hydrological properties and flow paths. Water Resour Res 41:W12419

Loope D, Swinehart J (2000) Thinking like a dune field: Geologic history in the Nebraska Sand Hills. Great Plains Res 10:5–35

Ludwig JA, Wilcox BP, Breshears DD, Tongway DJ, Imeson AC (2005) Vegetation patches and runoff-erosion as interacting ecohydrological processes in semiarid landscapes. Ecology 86:288–297

Miao X, Mason JA, Swinehart JB, Loope DB, Hanson PR, Goble RJ, Liu X (2007) A 10,000 year record of dune activity, dust storms, and severe drought in the central Great Plains. Geology 35:119–122

Rasse DP, Smucker A, Santos D (2000) Alfalfa root and shoot mulching effects on soil hydraulic properties and aggregation. Soil Sci Soc Am J 64:725–731

Rienzner M, Gandolfi C (2014) Investigation of spatial and temporal variability of saturated soil hydraulic conductivity at the field-scale. Soil Tillage Res 135:28–40

Schaap MG, Leij FJ (1998) Database-related accuracy and uncertainty of pedotransfer functions. Soil Sci 163:765–779

Schenk HJ, Jackson RB (2002) The global biogeography of roots. Ecol Monogr 72:311–328

Sitch S, Smith B, Prentice IC, Arneth A, Bondeau A, Cramer W, Kaplan JO, Levis S, Lucht W, Sykes MT, Thonicke K, Venevsky S (2003) Evaluation of ecosystem dynamics, plant geography and terrestrial carbon cycling in the LPJ dynamic global vegetation model. Glob Change Biol 9:161–185

Stephens DB (1996) Vadose Zone Hydrology. CRC Press, Lewis Publishers, New York

Wang TJ, Zlotnik VA, Wedin D, Wally KD (2008) Spatial trends in saturated hydraulic conductivity of vegetated dunes in the Nebraska Sand Hills: effects of depth and topography. J Hydrol 349:88–97

Wang TJ, Istanbulluoglu E, Lenters J, Scott D (2009a) On the role of groundwater and soil texture in the regional water balance: An investigation of the Nebraska Sand Hills, USA. Water Resour Res 45:W10413

Wang TJ, Wedin D, Zlotnik VA (2009b) Field evidence of a negative correlation between saturated hydraulic conductivity and soil carbon in a sandy soil. Water Resour Res 45:W07503

Wang TJ, Zlotnik VA, Simunek J, Schaap MG (2009c) Using pedotransfer functions in vadose zone models for estimating groundwater recharge in semiarid regions. Water Resour Res 45:W04412

Wang J, Bai Z, Yang P (2014a) Mechanism and numerical simulation of multicomponent solute transport in sodic soils reclaimed by calcium sulfate. Environ Earth Sci 72:1–13

Wang TJ, Chen X, Tang AM, Cui YJ (2014b) On the use of the similar media concept for scaling soil air permeability. Geoderma 235:154–162

Wilcox BP, Breshears DD, Turin HJ (2003) Hydraulic conductivity in a pinon-juniper woodland: influence of vegetation. Soil Sci Soc Am J 67:1243–1249

Williams CA, Albertson JD (2004) Soil moisture controls on canopy-scale water and carbon fluxes in an African savanna. Water Resour Res 40:W09302

Williams CA, Albertson JD (2005) Contrasting short- and long-timescales effects of vegetation dynamics on water and carbon fluxes in water-limited ecosystems. Water Resour Res 41:W06005

Wösten JHM, Pachepsky YA, Rawls WJ (2001) Pedotransfer functions: Bridging the gap between available basic soil data and missing soil hydraulic characteristics. J Hydrol 251:123–150

Yair A (2003) Effects of biological soil crusts on water redistribution in the Negev desert, Israel: A case study in longitudinal dunes. In: Belnap J, Lange OL (eds) Biological soil crusts: structure, function, and management, 2nd edn. Springer, Berlin, pp 303–314

Zhang WJ, Zhang GG, Chen YM (2013) Analyses on a high leachate mound in a landfill of municipal solid waste in China. Environ Earth Sci 70:1747–1752

Zhou Z, Wang J, Huang Y, Xu H (2014) Conceptual data model and method of settlement calculation for deformation and water release from saturated soft soil. Environ Earth Sci 71:4235–4245